Proceedings of the 16th European VLBI Network Symposium
Ros, E., Benke, P., Dzib, S., Rottmann, I., & Zensus, J.A. (eds.)
September 2nd-6th 2024, Bonn, Germany

Modelling the jet structure of the blazar NRAO 150 using mm-VLBI

L. C. Debbrecht, G. F. Paraschos, T. P. Krichbaum, E. Ros, and J. A. Zensus

Max-Planck-Institut für Radioastronomie, Auf dem Hügel 69, D-53121 Bonn, Germany

Abstract. NRAO 150 is a prominent radio loud quasar at redshift z = 1.52. This source exhibits a particularly intriguing structure, as the jet is seen at an extremely small angle to the line of sight (LOS). Previous Very Long Baseline Interferometry (VLBI) observations have revealed a fast counter-clockwise rotation of its innermost jet region. Owing to the high angular resolution provided by VLBI, we can probe relativistic jets at such small scales, in the vicinity of the central engine. In this work, we aim to study the morphology and kinematic behaviour of the jet of NRAO 150. The source was observed by the Global Millimeter VLBI Array (GMVA) between April 2021 and April 2022 at 86 GHz. The data was imaged in total intensity and geometric model fitting was applied, in order to perform a comprehensive analysis of the jet structure. We report a counter-clockwise jet rotation for one emission feature, which is consistent with previous VLBI studies. We also present a new kinematic model for this source and fit a helical model to the component's trajectory. The fit supports the assumption of a counter-clockwise jet rotation. Geometric projection effects also need to be taken into account, as the source points at a small angle to our line of sight. In this work we examine and discuss possible scenarios for these projection effects and interpret how they relate to the observed jet features.

1. Introduction

Blazars are the most luminous types of Active Galactic Nuclei (AGN), which exhibit an energetic jet emanating from the central region of a galaxy. A defining characteristic of blazars is that the jets are pointing at a small angle to our line of sight (LOS). Examining the physical properties of such jets is crucial in order to understand the mechanisms of jet formation and their kinematic behaviour.

NRAO 150 is a radio-mm blazar at redshift of 1.52 (Acosta-Pulido et al., 2010) and exhibits a prominent jet, pointing at a small angle to our LOS ($\phi \approx 8°$, Agudo et al., 2007). A past analysis of high-resolution data report an extremely fast counter-clockwise jet rotation with an angular speed up to $\approx 11\,° \,\mathrm{yr}^{-1}$ (Molina et al., 2014). In addition to this rotation, the inner jet structure shows a wobbling movement in the plane of the sky (Agudo et al., 2007). As the jet wobbling is observed in the innermost region of jets, Agudo et al. (2008) suggest that this phenomenon is connected to the region where the jet is emitted, that is the accretion disc. Molina et al. (2014) found that the motion of the jet emission features is non-ballistic and follows a helical path. The aforementioned jet kinematics are believed to be linked to the same phenomenon, but until today, there is no distinct physical process explaining this motion. Utilising the extreme features of this jet makes NRAO 150 an excellent source for investigating the physical origin of jet-kinematics.

2. Observations and Methods

We analysed three epochs of the blazar NRAO 150, observed by the GMVA at 86 GHz. Despite the constraints on the number of observations, these epochs provide a representative sample of the jet's motion profile. The choice of 86 GHz observations provides us with a resolution capable of detecting the inner jet structure, crucial for studying the jet kinematics of NRAO 150. The data was first calibrated using the new pipeline `rPICARD`[1] (Janssen et al., 2019) and the imaging was done using the `CLEAN`-algorithm (Högbom, 1974) in `DIFMAP`. The morphology and kinematics of the jet were characterised using total intensity images and geometric model fitting.

3. Total Intensity Images of NRAO 150

The `CLEAN`-images of NRAO 150 in total intensity at 86 GHz are shown in Fig. 1. These images were convolved with the same (circular) beam size of 0.09 mas, which was estimated based on the geometrical mean of major and minor axis. The colour scale indicates the total intensity, in which the contours indicate the contour levels of 1, 2, 4, 8, 16, 32, and 64 % of the peak flux density. The beam size is indicated in blue in the bottom left corner and the blue dash in the right corner corresponds to the (projected) distance in parsec. The white crosses indicate the position of the fitted `MODELFIT`-components and the circles indicate their size, in which the diameter is equal to the Full Width at Half Maximum (FWHM) of the fitted circular Gaussians. We will denote the core component as C0, the two components along the jet as C1 and C2, and the component in the south and north from the core in April 2021

[1] Comparative tests demonstrate that `rPICARD` produces results consistent with AIPS analysis, as shown in its application presented in Kim et al. (2023).

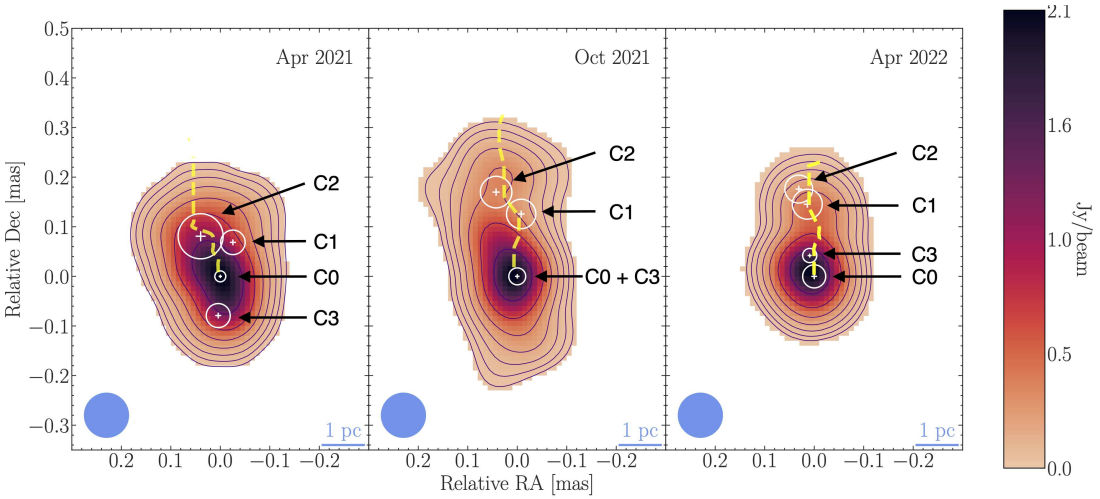

Fig. 1. Total intensity images of NRAO 150 at 86 GHz. The total intensity flux density is represented by the contours, using the contour levels at 1, 2, 4, 8, 16, 32, and 64% of the peak flux. The blue circle in the bottom left corner denotes the convolving, circular beam with a size of 0.09 mas for all three epochs. The peak flux density of the first epoch is 0.22 Jy/beam, 0.55 Jy/beam for the second, and 1.40 Jy/beam for the third epoch. The cut-off is at $1\,\sigma_{\rm I}$ for the first epoch, $2\,\sigma_{\rm I}$ for the second, and $3\,\sigma_{\rm I}$ for the last epoch. The blue dash in the bottom right corner corresponds to the projected distance in parsec.

	April 2021		October 2021		April 2022	
Component	RA	Dec	RA	Dec	RA	Dec
C0 (+ C3)	0.00	0.00	0.00	0.00	0.00	0.00
C1	-0.03 ± 0.02	0.07 ± 0.02	-0.01 ± 0.01	0.13 ± 0.01	0.02 ± 0.01	0.15 ± 0.01
C2	0.04 ± 0.01	0.10 ± 0.01	0.04 ± 0.01	0.20 ± 0.01	0.03 ± 0.01	0.18 ± 0.01
C3	0.01 ± 0.01	-0.08 ± 0.01	-	-	0.01 ± 0.01	0.04 ± 0.01

Table 1. Positions in RA and Dec in mas of the `MODELFIT`-components of all three epochs, which were determined using the position of the fitted circular Gaussians in polar-coordinates.

and 2022 as C3. The positions of the fitted `MODELFIT`-components of all three epochs are listed in Table 1.

The images in total intensity are crucial for identifying the positions of the jet components, enabling us to trace the motion of emission features over time. By examining the morphology in these total intensity maps, we can track patterns in jet evolution, providing information about the jet formation process. In order to model the trajectory of the emission features and examine how the jet of NRAO 150 is launched, we used the `MODELFIT`-components and performed kinematic analysis, which are discussed in the next section.

4. A new kinematic model for NRAO 150

The images in total intensity in Fig. 1 indicate, that the components C1 and C2 recede from the core with increasing epoch. In order to analyse this kinematic pattern in more detail, we plotted the position of all components C1, C2, and C3 in Fig. 2 for all three epochs, similar to what is presented in Molina et al. (2014). In this case, we consider component C0 to be the stationary VLBI core. Component C1 is plotted in blue, C2 in red, and C3 in green, with the colour gradually becoming lighter with increasing epoch for all components. The plot in Fig. 2 shows, that the trajectory appears to be bent and non radial for C1 and C3, as the radial distance increases with increasing epoch. As a consequence, we can conclude that the jet features, represented with C1 and C3, follow a non-ballistic and bent motion. For C2, the movement seems to be straight within the error budget. Here, we present a new kinematic model describing the motion of the jet emission of NRAO 150, which is based on the model presented in Molina et al. (2014): We assume that the magnetic field threading the innermost jet region follows a helical structure. Material escaping from the rotating accretion disc is dragged along the twisted magnetic field lines and follows the bent structure. Therefore, the emission features are rotating around the jet axis on a helical path, whereby the axis of rotation corresponds to the axis of the helix. The emission features represented by the `MODELFIT`-components can be explained by boosted features, that move in the direction towards our LOS. Figure 3 depicts the schematic representation of this new model, in which the left side of Fig. 3 depicts the new model when it is seen from a high elevation. Since NRAO 150 is pointing

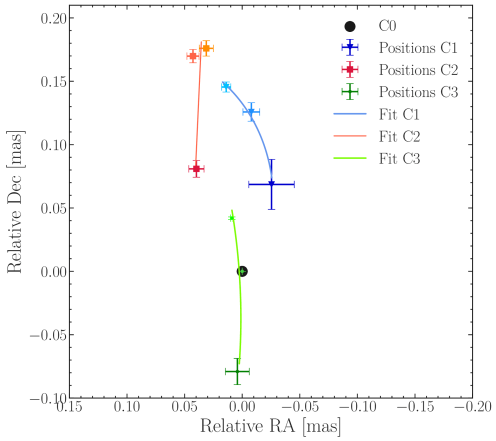

Fig. 2. Fit of the MODELFIT-components throughout the observed epochs for C1, C2 and for C3. C1 is depicted in blue, C2 in red, and C3 in green, in which the colour gradient increases with increasing epoch. For its calculation the core component C0 is considered to be stationary at (0,0) and the errors for the position are calculated as described in Jorstad et al. (2017).

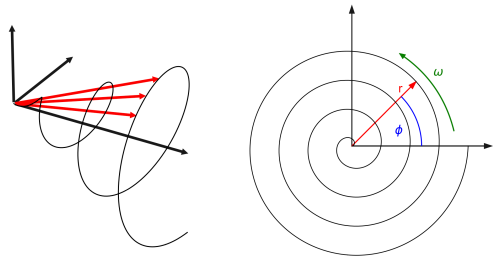

Fig. 3. Graphical representation of the new model using a helical trajectory of the emission feature. The red arrow denotes the distance r from the core component C0 to the components of each epoch. The right plot shows the trajectory when it is seen face-on, showing the projected distance r. The green arrow denotes the direction of the angular velocity ω.

with a small angle to the LOS, the resulting trajectory of the helical path is described by a spiral, which is shown on the right in Fig. 3. The trajectory of each component can be parameterised in Cartesian coordinates using

$$x(t) = (v_\mathrm{j}^\mathrm{r} t + c)\cos(\omega_\mathrm{j} t) \quad (1)$$
$$y(t) = (v_\mathrm{j}^\mathrm{r} t + c)\sin(\omega_\mathrm{j} t), \quad (2)$$

in which c is a constant and t the time over the interval from 0 to 1. The parameter ω_j denotes the projected angular velocity and v_j^r denotes the projected radial velocity for the motion of the j-th component.
We analysed the motion of components C1 and C3 by fitting these functions to the positions of the MODELFIT-components in Fig. 2. As a result, the fitted radial and angular velocity read:

$$v_\mathrm{C1}^\mathrm{r} = (0.01 \pm 0.01)\,\mathrm{mas/yr}$$
$$\omega_\mathrm{C1} = (-42 \pm 8.0)\,\mathrm{deg/yr}$$
$$v_\mathrm{C3}^\mathrm{r} = (-0.01 \pm 0.01)\,\mathrm{mas/yr}$$
$$\omega_\mathrm{C3} = (-15 \pm 7.0)\,\mathrm{deg/yr},$$

in which the parameter c was negligibly small.
From the fit parameters we see that the radial angular separation rates for both components C1 and C3 are within the measurement error not distinguishable. The angular velocities differ by a factor of almost 3. For component C2, however, the counter-clockwise spiral fit did not produce a reasonable reduced χ^2 value. We therefore tested a linear fit using the relation $y = m \cdot x + b$, in which m is the slope and b the intersection with the y-axis. The fit parameters for the linear fit for component C2 are:

$$m_\mathrm{C2} = (20 \pm 1)\,\mathrm{mas/yr} \quad b_\mathrm{C2} = (-0.90 \pm 0.03)\,\mathrm{mas}. \quad (3)$$

Nevertheless, the positive slope indicates that the movement of C2 is directed in the opposite direction, as for the movement represented by C1 and C3. Since it is energetically very unlikely that one emission feature is moving against the direction of the other emission features, there is a need to examine possible scenarios to explain this behaviour. In the next section, we will discuss two possible scenarios for the trajectory of the emission features, in order to explain the jet dynamics of NRAO 150.

4.1. Scenario 1: Two Filaments

From Fig. 2 it appears that the components C1, C2, and C3 are following separate filament-like trajectories. In the context of a relativistic jet, this pattern can be attributed to a filamentary structure of the jet's emission features. It is therefore straightforward to conclude that one possible scenario for the trajectory includes helical filaments. This scenario is schematically shown in Fig. 4, in which the helical filaments are represented by the blue stripes. Fuentes et al. (2023) suggest, that these filaments are produced by plasma instabilities, such as current-driven (CD) kink or Kelvin-Helmholtz (KH) instabilities. These instabilities perturb the surrounding plasma in the accretion disc and can evolve into helical filamentary structures (Mizuno et al., 2012). The CD kink instability dictates the region where the jet's acceleration and collimation takes place, which is dominated by Poynting-flux areas of strong helical magnetic fields. The KH instability, however, outweighs for kinetically dominated flows. In the case of the jet in NRAO 150, both previously mentioned instabilities are possible explanations for its kinematics.
Referring back to the plot in Fig. 2 and invoking the aforementioned possible phenomena, the trajectories of C1, C2, and C3 can be described by separate helical filamentary structures. We suggest that C1, C2, and C3 are boosted features, that move on the filamentary structure, towards our LOS. As a consequence, the linear movement of C2 can be explained by the projection of the helical movement of the filamentary jet structure.

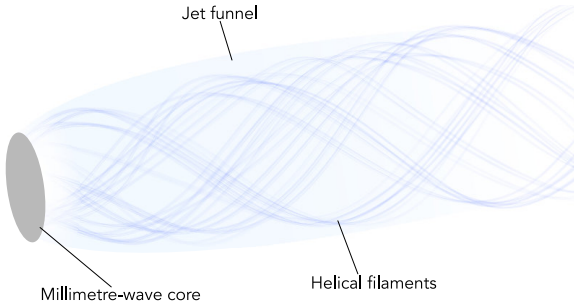

Fig. 4. Graphical representation of the new model for the internal structure of the jet NRAO 150, when it is seen at a larger angle to the LOS. The plasma is moving in a filamentary structure on a helical trajectory.

4.2. Scenario 2: Internal Jet Precession

As observed by Agudo et al. (2007) and Agudo et al. (2008), NRAO 150 shows an additional internal jet precession, which is also known as jet-wobbling. Tchekhovskoy et al. (2014) suggest that the jet-wobbling phenomenon is a phase of violent rearrangement triggered by a magnetically arrested disk (MAD) (Narayan et al., 2003): At some point, the magnetic field reaches a stage where it is sufficiently strong to interact with the accretion disc. They further assert that the interaction causes the rotation axis of the jet to align with the spin axis of the black hole. During this process, the jet wobbles intensively between these two axis. As a consequence, the emission features change its appearance with the erratic motion of the jet, which also changes their arrangement in the images.
In this scenario we include the phenomenon of jet-wobbling to describe the motion of the inner jet region. To support the aforementioned scenario, we performed a ridge line fitting as in Paraschos et al. (2022) to all three epochs. The ridge line is defined by the peak of the 1D Gaussians fitted at each slice perpendicular to the jet direction and provides information about the bulk flow of the jet. Figure 1 shows the ridge line as yellow dashed lines in every epoch. We omit the error bars for the ridge line in these plots to improve the readability of the diagram and assume an uncertainty of 1/5 of the (nominal) beam size. The ridge lines indicate that the bulk jet flow is directed to the north and exhibits a bend at around 0.1 mas. However, we want to stress that due to the uncertainty of the ridge line, its detailed shape needs further investigation, ideally with future images of higher dynamic range.

5. Conclusions

Our conclusions can be summarised as follows:

- Observations at 86 GHz reveal a complex jet morphology in the blazar NRAO 150, with three prominent emission features tracked across all epochs.
- We examined a new kinematic model for NRAO 150 by fitting a helical model to the jet feature trajectories, indicating a counter-clockwise rotation in the innermost region.
- We examined two kinematic models considering projection effects and interpreted how they relate to the observed jet features. In the first scenario, each feature travels along a separate helical filament, while the observed linear movement of C2 resulting from a projection effect caused by its helical motion. The second scenario is based on the presence of an internal jet precession of the innermost region in NRAO 150.
- Although this analysis provides valuable insights, a comprehensive kinematic study is ideally based on a larger data set, as kinematic studies are sensitive to minor trajectory variations. Utilising additional epochs will allow for a more robust and detailed characterisation of the helical parameters.

Acknowledgements. This research has made use of data obtained using the Global Millimetre VLBI Array (GMVA), which consists of telescopes operated by the Max-Planck-Institut für Radioastronomie (MPIfR), IRAM, Onsala, Metsähovi Radio Observatory, Yebes, the Korean VLBI Network, the Greenland Telescope, the Green Bank Observatory (GBT) and the Very Long Baseline Array (VLBA). The GLT is part of the ALMA–Taiwan project and is supported in part by the Academia Sinica (AS) and the Ministry of Science and Technology of Taiwan. This publication acknowledges project M2FINDERS, which is funded by the European Research Council (ERC) under the European Union's Horizon 2020 research and innovation programme (grant agreement no. 101018682).

References

Acosta-Pulido, J. A., Agudo, I., Barrena, R., et al. 2010, A&A, 519, A5
Agudo, I., Bach, U., Krichbaum, T. P., et al. 2008, in Astronomical Society of the Pacific Conference Series, Vol. 386, Extragalactic Jets: Theory and Observation from Radio to Gamma Ray, ed. T. A. Rector & D. S. De Young, 249
Agudo, I., Bach, U., Krichbaum, T. P., et al. 2007, A&A, 476, L17
Fuentes, A., Gómez, J. L., Martí, J. M., et al. 2023, Nature Astronomy, 7, 1359
Högbom, J. A., A&AS, vol. 15, pp. 417, June 1974
Janssen, M., Goddi, C., van Bemmel, I. M., et al. 2019, A&A, 626, A75
Jorstad, S. G., Marscher, A. P., Morozova, D. A., et al. 2017, ApJ, 846, 98
Kim, D.-W., Janssen, M., Krichbaum, T. P., et al. 2023, A&A, 680, L3
Mizuno, Y., Lyubarsky, Y., Nishikawa, K.-I., & Hardee, P. E. 2012, The Astrophysical Journal, 757, 16
Molina, S. N., Agudo, I., Gómez, J. L., et al. 2014, A&A, 566, A26
Narayan, R., Igumenshchev, I. V., & Abramowicz, M. A. 2003, PASJ, 55, L69
Paraschos, G. F., Krichbaum, T. P., Kim, J. Y., et al. 2022, A&A, 665, A1
Tchekhovskoy, A., Metzger, B. D., Giannios, D., & Kelley, L. Z. 2014, MNRAS, 437, 2744